HOSTED BY

Available online at www.sciencedirect.com
ScienceDirect
Journal of Radiation Research and Applied Sciences
journal homepage: http://www.elsevier.com/locate/jrras

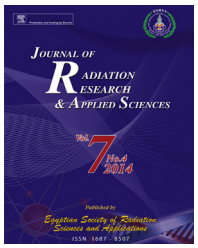

# UV and gamma ray induced thermoluminescence properties of cubic $Gd_2O_3:Er^{3+}$ phosphor

*Raunak Kumar Tamrakar* [a,*], *Durga Prasad Bisen* [b], *Ishwar Prasad Sahu* [b], *Nameeta Brahme* [b]

[a] *Department of Applied Physics, Bhilai Institute of Technology (Seth Balkrishan Memorial), Near Bhilai House, Durg (C.G.) 491001, India*
[b] *School of Studies in Physics and Astrophysics, Pt. Ravishankar Shukla University, Raipur (C.G.) 492010, India*

ARTICLE INFO

*Article history:*
Received 16 June 2014
Accepted 8 July 2014
Available online 30 July 2014

*Keywords:*
Thermoluminescence
Gamma irradiation
UV irradiated
TL dosimetry
Activation energy
Order of kinetics
Frequency factor

ABSTRACT

This paper reports the thermoluminescence properties of $Er^{3+}$ doped gadolinium oxide nanophosphor. The phosphor is prepared by high temperature solid state reaction method. The method is suitable for large scale production. Starting materials used for sample preparation were $Gd_2O_3$, $Er_2O_3$ (0.5–2.5 mol%) and fixed concentration of boric acid using as a flux. The prepared samples were characterized by X-ray diffraction technique and the particle size calculated by Scherer's formula. The surface morphology of prepared phosphor is determined by scanning electron microscopic (SEM) technique. Functional group analysis was done by Fourier transform infra-red spectroscopy (FTIR) analysis. The elemental analysis of prepared sample was determined by energy dispersive X-ray analysis (EDX) and the exact particle size of prepared phosphor for the different concentration of dopant ($Er^{3+}$) was evaluated by transmission electron microscopy (TEM) technique. The prepared phosphors for different concentration of $Er^{3+}$ were examined by thermoluminescence (TL) glow curve for UV and gamma irradiation. The UV 254 nm source was used for UV irradiation and $Co^{60}$ source was used for gamma irradiation. The samples show well resolved broad peak covered the temperature range 50–250 °C and the peak temperature found at 126 °C for UV irradiation and higher temperature peak at 214 °C for gamma irradiation. The effect of heating rate on TL studies was presented for optimized sample. Here UV irradiated sample shows the formation of shallow trap (surface trapping) and the gamma irradiated sample shows the formation of deep trapping. The estimation of trap formation was evaluated by knowledge of trapping parameters. The trapping parameters such as activation energy, order of kinetics and frequency factor were calculated by peak shape method. Here most of the peak shows second order of kinetics. The effect of gamma and UV exposure on TL studies was also examined and it shows linear and sublinear response with dose which indicates that the sample may be useful for TL dosimetry.


* *Corresponding author*. Tel.: +91 9827850113.
E-mail addresses: raunak.ruby@gmail.com, raunak.physics@gmail.com (R.K. Tamrakar).
Peer review under responsibility of The Egyptian Society of Radiation Sciences and Applications.
http://dx.doi.org/10.1016/j.jrras.2014.07.003

## 1. Introduction

Thermoluminescence (TL) has been widely used as a mechanism to explain the nature of electron traps and trapping processes in excited phosphors, which is semiconductor or insulator. Basically it is the emission of photon in the form of light from a solid, inorganic material, when it is heated after its exposure to some radiation such as α, β, γ, X-ray or UV radiation etc. This energy is stored in a phosphor due to excitation of electrons. The plot of the intensity of this emitted light vs temperature is known as the TL glow curve. The glow curves obtained for each natural or synthetic phosphor were different, and each glow peak is ascribed to the recombination centres and is related to the traps. It can be used for estimating the activation energy 'E' for the thermal release of the trapped electrons or holes and provides means of determining the escape frequency factor S (Vij, 1993).

The synthesis and development of new generation phosphors that exhibit tremendous TL response with higher stability and having potential to be used in detectors and dosimeters application is a great challenge for us (Barghare, Joshi, Kathuria, & Joshi, 1982; Noh, Amin, Mahat, & Bradley, 2001). TL depends on so many factors such as the crystal structure, band gap, synthesis process, crystal size, lattice imperfections and mainly the effects of impurities of solids. Lattice imperfections described as defect centres that may occur when ions of either signs move away from their original sites, thus leaving vacant sites that are able to interact with free charge carriers.

Aspects of TL have been widely studied in various theoretical as well as experimental applications upto present date specially for the developing dosimetry applications technique (Gokce, Oguz, Karali, & Prokic, 2009; Lawless, Chen, & Pagonis, 2009; Salah, Sahare, & Rupasov, 2007; Weiss, Horowitz, & Oster, 2008). TL has been demonstrated to be a trustworthy technique for different kinds of traps detectors in semiconductors or insulator materials and dosimeters applications. It is an important and convenient method for investigating, nature of traps, depth of traps and trapping levels present in different kind of solids (Falcony, Garcia, Ortiz, & Alonso, 1992; Mckeever, 1986). Different kinds of phosphor materials having TL property, means they emit light (in the form of photons) that can be best described by a TL glow curve.

Different types of TL materials have been reported, synthesized by traditional approaches to modify the crystal structure (band structure) of the phosphor as well as the characteristics of their electron traps, thus controlling the TL response of it. On the other side, size effects on the TL properties of phosphors remain very much an open area for investigating new phenomenon or concept of these mechanisms (Chen & Kirsh, 1981; Tiwari, Khan, Kher, Dhoble, & Mehta, 2011). Currently phosphor in nano sized has attracted several researches from different fields of materials and bioscience, especially, from the field of luminescence (Nalwa, 2000). It has been found that the physical and optical properties of individual nano range phosphor materials can be different from those of their bulk counterparts (Tamrakar, 2012, Tamrakar & Bisen, 2013; Tamrakar, Bisen, & Brahme, 2014; Tamrakar, Bisen, Robinson, Sahu, & Brahme, 2014). Recent studies on different luminescent nanomaterials have showed that they have potential application in dosimetry of ionizing radiations for the measurement of high doses using the TL technique, where the conventional microcrystalline phosphors saturate (Lochab, Pandey, et al., 2007; Lochab, Sahare, et al., 2007; Sahare, Ranjan, Salah, & Lochab, 2007 Salah, Sahare, Lochab, & Kumar, 2006; Salah et al., 2007).

The present study shows the effect of $Er^{3+}$ concentration on TL properties of $Gd_2O_3$ phosphor prepared by solid state method. The prepared phosphors are nanocrystalline in nature and its TL behaviour compared to other commercially available phosphor was studied. The sample shows cubic structure and the TL glow curves show well resolved single peak for both UV and gamma irradiation. The effect of different exposure time of UV and gamma is also interpreted. Effect of heating rate on TL studies was carried out and the calculations of trap parameters were also interpreted by peak shape method.

## 2. Solid state synthesis of $Gd_2O_3:Er^{3+}$ phosphor

$Gd_2O_3:Er^{3+}$ phosphors were synthesized by conventional solid state method. Oxide of rare earth materials such as

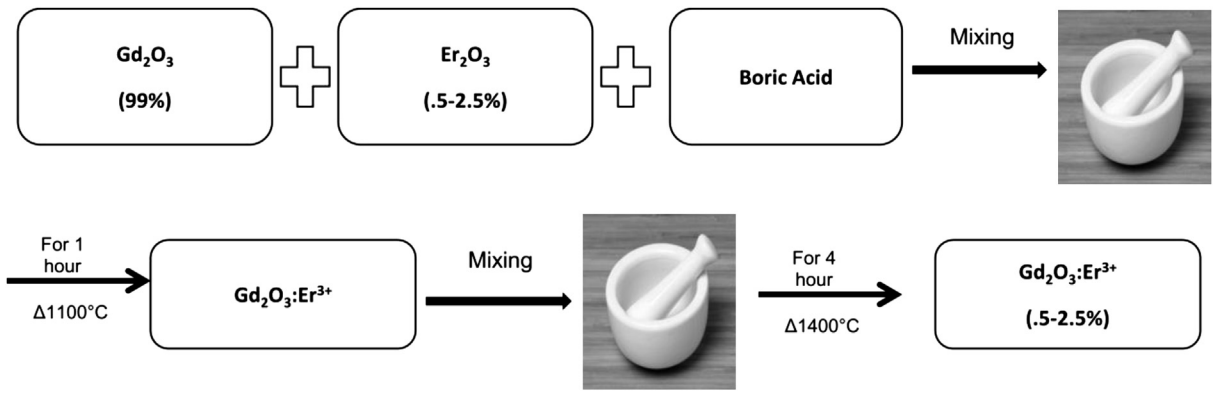


**Scheme 1 – Synthesis of $Er^{3+}$ doped $Gd_2O_3$ phosphor.**

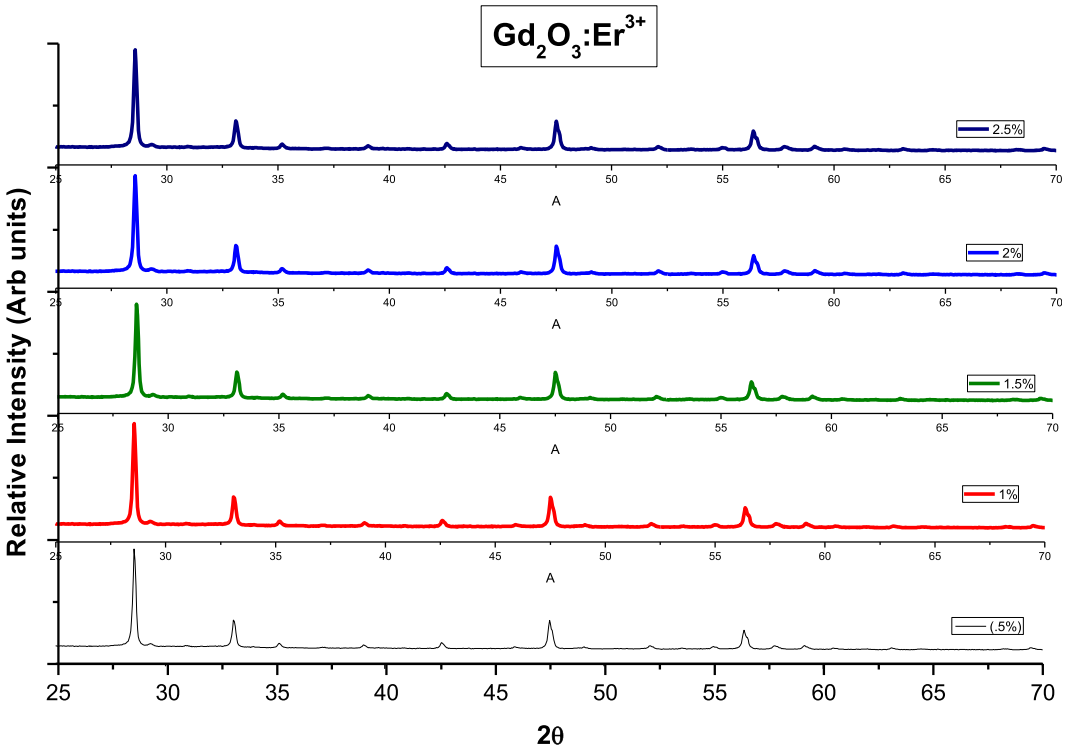


**Fig. 1 – XRD patterns of $Gd_2O_3$:$Er^{3+}$(0.5–2.5%) phosphor.**

Gadolinium Oxide ($Gd_2O_3$), Erbium Oxide ($Er_2O_3$) and Boric Acid as a flux with high purity (99.99%) were used as precursor materials to prepare $Er^{3+}$ doped $Gd_2O_3$ phosphor. In stoichiometric ratios of rare earth ions $Er^{3+}$(0.5–2.5 mol%) and $Gd_2O_3$ were used to synthesize $Gd_2O_3$:$Er^{3+}$ phosphor with different mol% of $Er^{3+}$ ion. These chemicals were weighed and grinded into a fine powder by using agate mortar and pestle. The grinded sample were placed in an alumina crucible and

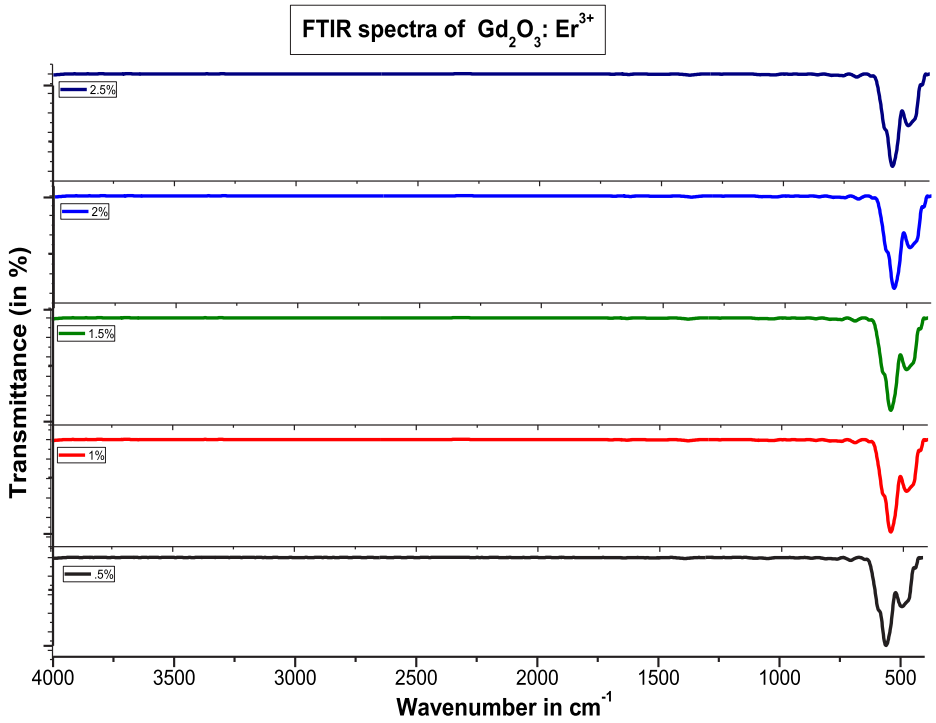


**Fig. 2 – FTIR spectra of $Gd_2O_3$:$Er^{3+}$(0.5–2.5%) phosphor.**

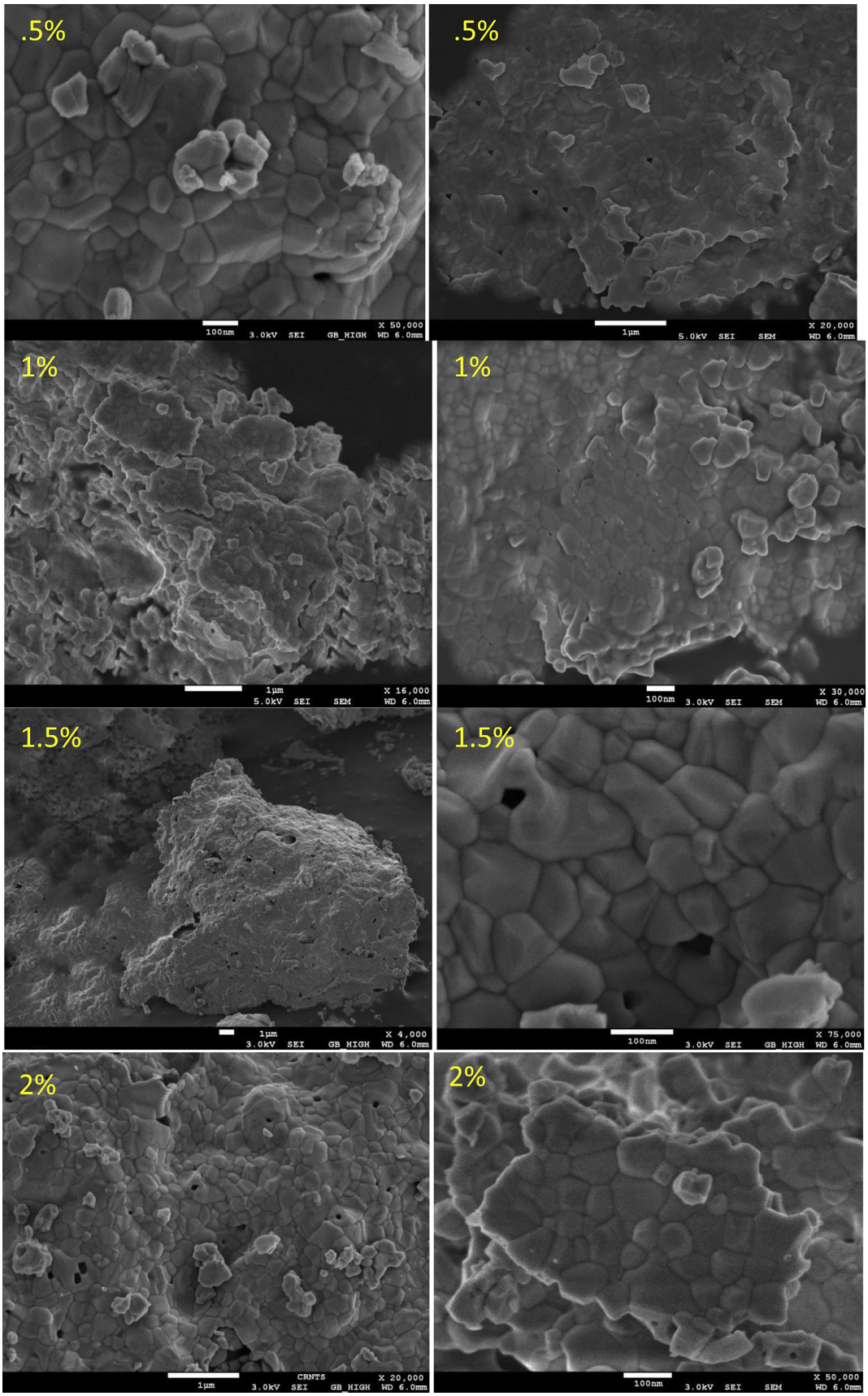


**Fig. 3 – Scanning electron microscope images of $Gd_2O_3:Er^{3+}$ phosphor.**

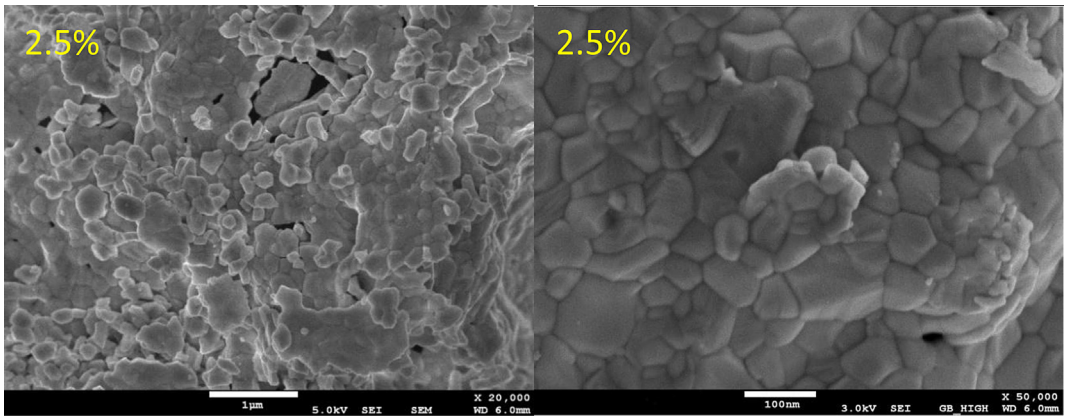


**Fig. 3 – (*continued*).**

heated at 1100 °C for 1 h followed by dry grinding and further heated at 1400 °C for 4 h in a muffle furnace. The sample is allowed to cool at room temperature (Scheme 1) All the prepared phosphors were ground by mechanical grinding for same duration. (Kaur, Parganiha, Dubey, & Singh, 2014; Mahajna & Horowitz, 1997; Singh, Chopra, & Lochab, 2011; Tamrakar, Bisen, Sahu, & Brahme, 2014; Tiwari et al., 2014).

## 3. Characterization of prepared phosphor

Crystalline phases and sizes of prepared phosphors were characterized by powder X-ray diffraction (XRD; Bruker D8 Advance). The X-rays were produced using a sealed tube and the wavelength of X-ray was 0.154 nm (Cu K-alpha). The X-rays were detected using a fast counting detector based on Silicon strip technology (Bruker Lynx Eye detector). The particle size was calculated using the Scherer formula. The morphology and particle size of $Gd_2O_3$:$Er^{3+}$ phosphor were observed by transmission electron microscopy (TEM) (Philips CM-200), and field emission-scanning electron microscope (FE-SEM) (JSM-7600F). TL glow curve were recorded at room temperature by using TLD reader I1009 (Nucleonix Sys. Pvt. Ltd. Hyderabad). The obtained phosphor under the TL examination is given UV radiation using 365 nm UV source, and gamma irradiation using $Co^{60}$ source (Tamrakar & Bisen, 2013; Tamrakar, Bisen, & Brahme, 2014; Tamrakar, Bisen, Robinson, et al., 2014). All of the measurements were performed at room temperature.

### 3.1. *XRD results*

The XRD patterns of the samples are shown in Fig. 1. It shows a cubic structure match with JCPDS card no. 43-1014 (Grier & Mccarthy, 1991). The XRD peaks correspond to Bragg diffraction at (111), (200), and (220), (311) and (222) planes of face centred cubic $Gd_2O_3$. The width of the peak is directly related to the particle size. The width increases as the size of the particle decreases and increased as width decreased. The size of the particles has been computed from the full width half maximum (FWHM) of the intense peak using the Scherer formula.

$$D = 0.9\lambda/\beta \cos\theta$$

here $D$ is particle size, $\beta$ is FWHM (full width half maximum), $\lambda$ is the wavelength of X ray source; $\theta$ is angle of diffraction.

Diffraction angle, crystallite size and FWHM of prepared phosphors were presented in Table 1. There is small variation in particle size was found with increasing dopant ion concentration.

**Table 1 – Summary of diffraction angle, crystallite size and FWHM of prepared phosphor.**

| S. No. | $Er^{3+}$in percent | 2$\theta$ [°2Th.] | Intensity [cts] | FWHM [°2Th.] | $D$ (particle size) |
|---|---|---|---|---|---|
| 1. | 0.5 | 28.53 | 92,832 | 0.22 | 36.85 nm |
| | | 33.11 | 14,056 | 0.23 | 35.64 nm |
| | | 47.54 | 12,384 | 0.24 | 35.77 nm |
| | | 56.70 | 26,897 | 0.25 | 35.71 nm |
| 2. | 1 | 28.57 | 91,904 | 0.19 | 42.67 nm |
| | | 33.07 | 13,915 | 0.19 | 43.13 nm |
| | | 45.54 | 12,260 | 0.20 | 42.60 nm |
| | | 56.36 | 26,628 | 0.21 | 42.44 nm |
| 3. | 1.5 | 28.53 | 97,474 | 0.17 | 47.69 nm |
| | | 33.13 | 14,759 | 0.17 | 48.22 nm |
| | | 45.54 | 13,003 | 0.18 | 47.24 nm |
| | | 56.46 | 28,242 | 0.19 | 46.93 nm |
| 4. | 2 | 28.55 | 92,732 | 0.16 | 50.67 nm |
| | | 33.17 | 13,956 | 0.15 | 54.65 nm |
| | | 45.54 | 12,284 | 0.15 | 56.80 nm |
| | | 56.22 | 26,797 | 0.16 | 55.67 nm |
| 5. | 2.5 | 28.54 | 93,332 | 0.14 | 57.91 nm |
| | | 33.15 | 14,556 | 0.14 | 58.55 nm |
| | | 45.54 | 12,884 | 0.15 | 58.80 nm |
| | | 56.54 | 27,397 | 0.16 | 55.75 nm |

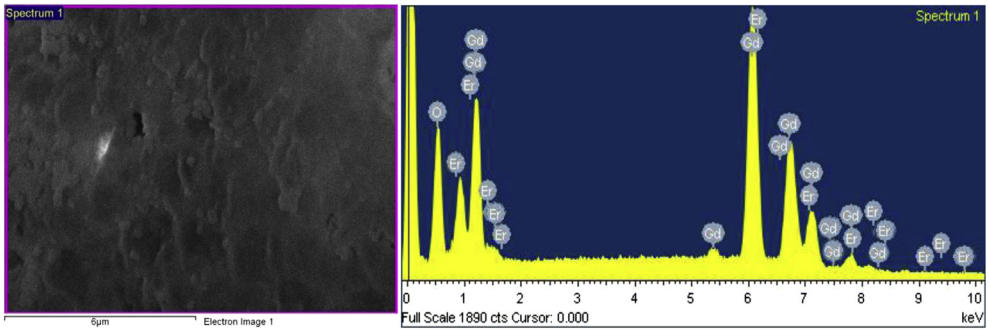


**Fig. 4 – EDX image of $Gd_2O_3:Er^{3+}$ phosphor.**

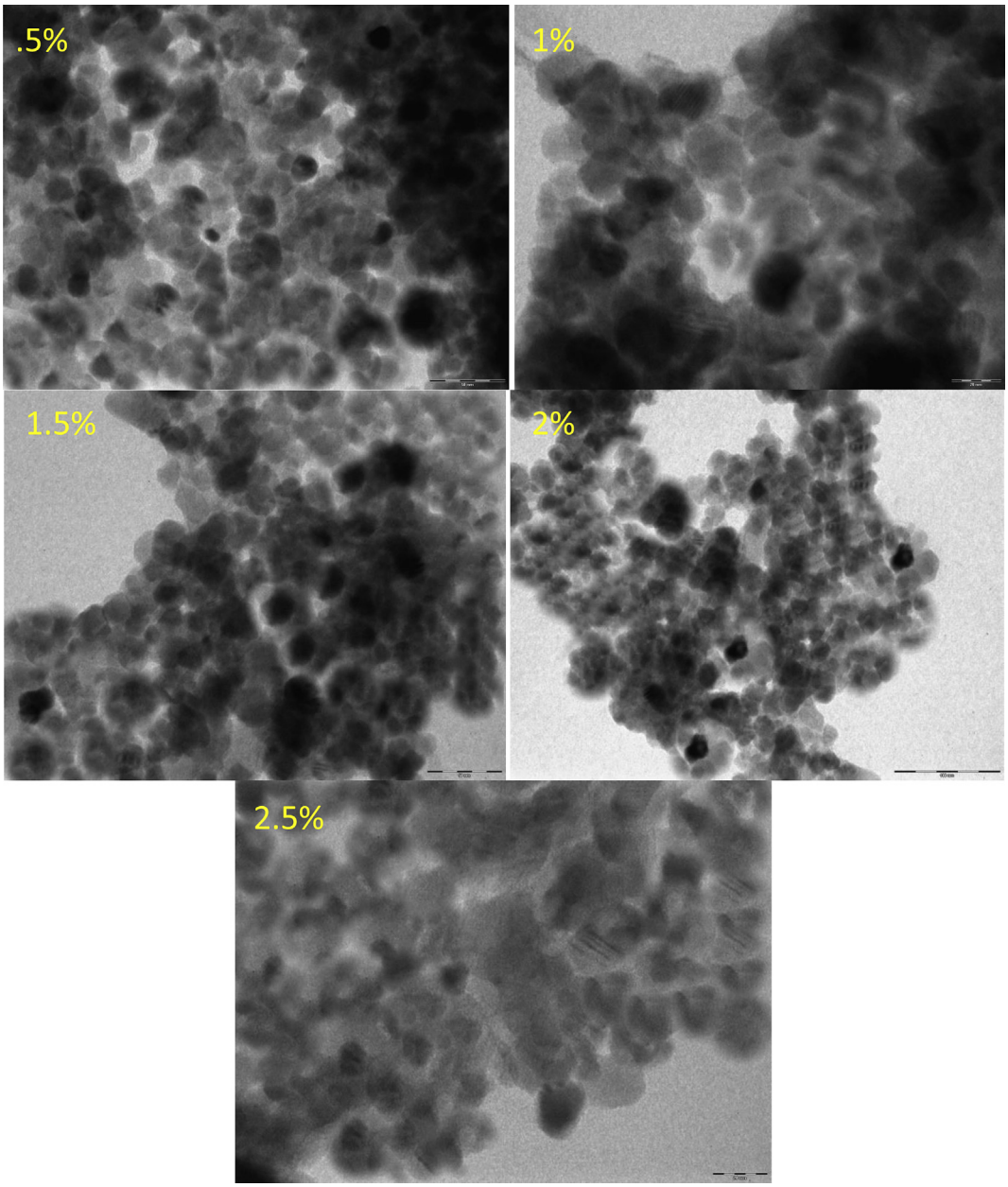


**Fig. 5 – TEM image of $Gd_2O_3:Er^{3+}$ phosphor.**

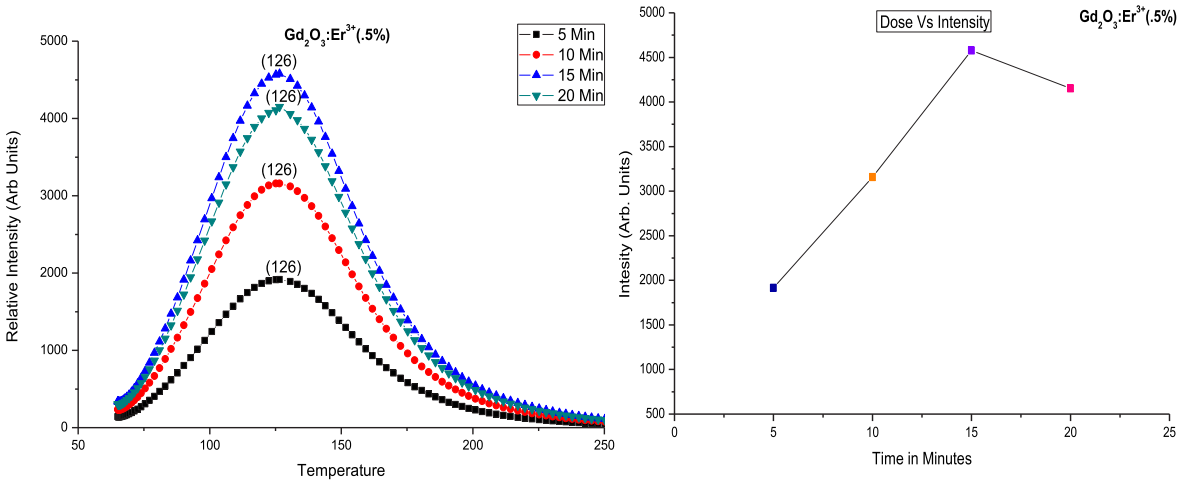


**Fig. 6 – TL glow curve of $Gd_2O_3:Er^{3+}$(0.5%) for different UV exposure time with heating rate 6.7 °C/s.**

### 3.2. *Fourier transform infra-red spectroscopy (FTIR) results*

The bands around 545 and 455 $cm^{-1}$ were assigned to the Gd–O vibration of $Gd_2O_3$, which is in agreement with others (Garcia-Murillo et al., 2002). These band confirms the formation of the $Gd_2O_3$. Vibration of this entire discussed peak confirms the formation of $Er^{3+}$ doped $Gd_2O_3$ phosphor. On the other hand, $Gd_2O_3$ shows weaker stability against atmospheric $CO_2$ and $H_2O$, which are known as luminescence killers (Guo et al., 2004). This is an advantage of solid state reaction synthesis, no band intensity of $CO_2$ and $H_2O$ were observed, which means it show very good luminescence intensity. Therefore, it is always of great interest to increase the luminescent properties of $Gd_2O_3$-based phosphor materials (Fig. 2).

### 3.3. *Field emission gun scanning electron microscopy (FEGSEM)*

The surface morphology of prepared phosphor were represented by FEGSEM images (Fig. 3). From SEM images it is concluded that the prepared phosphor shows nanocrystalline behaviour and good connectivity with grain which shows that powder size and morphology are well controlled. No significant difference is observed in XRD patterns and SEM micrographs. Some cracks and agglomerate are present in SEM image. the formation of cracks and agglomerate are due to high temperature synthesis method used for preparation of phosphor. For the variable concentration of $Er^{3+}$ the FEGSEM images show better connectivity with grains for 2 mol% of $Er^{3+}$.

### 3.4. *Energy dispersive X-ray analysis (EDX)*

Prepared sample is analysed by energy dispersive X-ray analysis to obtain the chemical composition of the prepared materials. In the spectrum intense peak of Gd, Er and O are present which confirm the formation of $Gd_2O_3:Er^{3+}$ phosphor (Fig. 4).

### 3.5. *Transmission electron microscopy (TEM) analysis*

Figure 5 displayed the HRTEM images of samples prepared under different resolutions. All these samples exhibited a sphere-like morphology with the particle size of about 5–47 nm. This two-dimensional growing habit coincided with the concept of preferential nucleation in this system, when the particle size continued to increase, a regular morphology of hexagonal flake was also observed, indicating that the crystals were better crystallized. These images are in very good agreement with XRD and FEGSEM results. It clearly shows the formation of nanosphere (Fig. 5).

## 4. Thermoluminescence results

### 4.1. *For different UV exposure time*

Fig. 6 shows TL glow curve for 0.5 mol% $Er^{3+}$ doped $Gd_2O_3$ phosphor with different UV exposure time at constant heating rate i.e., 6.7 °C $s^{-1}$. The sample shows resolved peak at 126 °C and linear response with dose up to 15 min UV exposure time after that the peak intensity decreases with increasing UV exposure time. This result shows the prepared phosphor may be useful for UV dosimetry application.

The dependence of the TL intensity on the irradiation time of the $Gd_2O_3:Er^{3+}$ sample from 5 to 20 min for all the $Er^{3+}$ concentration is shown in Figs. 6–10. The TL intensity increases as the irradiation time increases for all the concentration; this increase is mainly associated with the glow peak located at 126 °C. In this case, the weak glow peak at lower temperature however, it shows unstable behaviour and is ascribed to a trapping centre formed by a $Gd^{3+}$ ion and a defect complex formed from an oxygen vacancy and an anion. The corresponding kinetic parameters evaluated was shown in

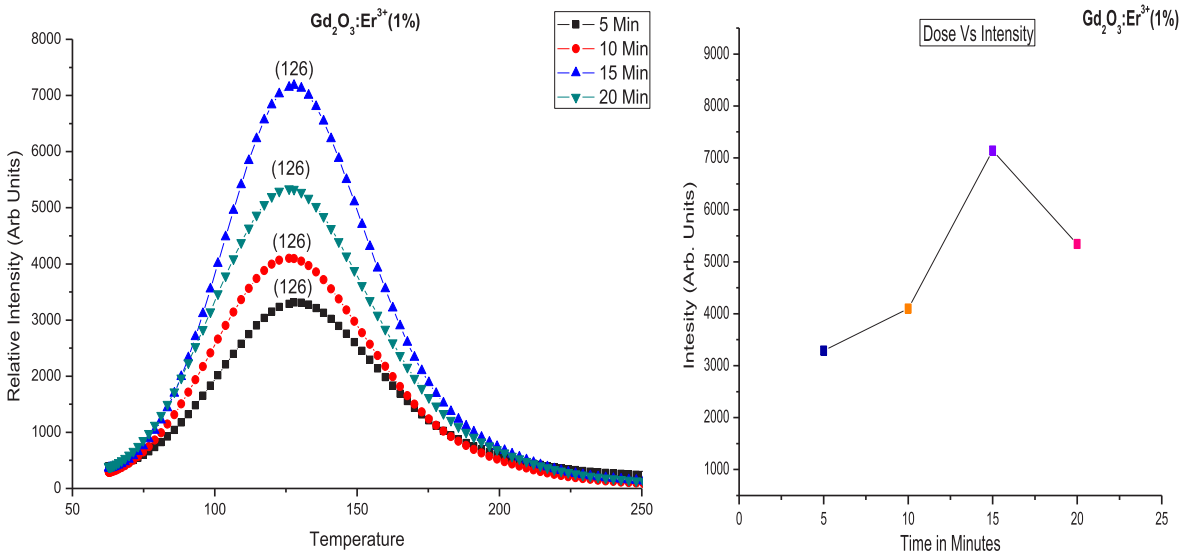


**Fig. 7 – TL glow curve of $Gd_2O_3:Er^{3+}$(1%) for different UV exposure time with heating rate 6.7 °C/s.**

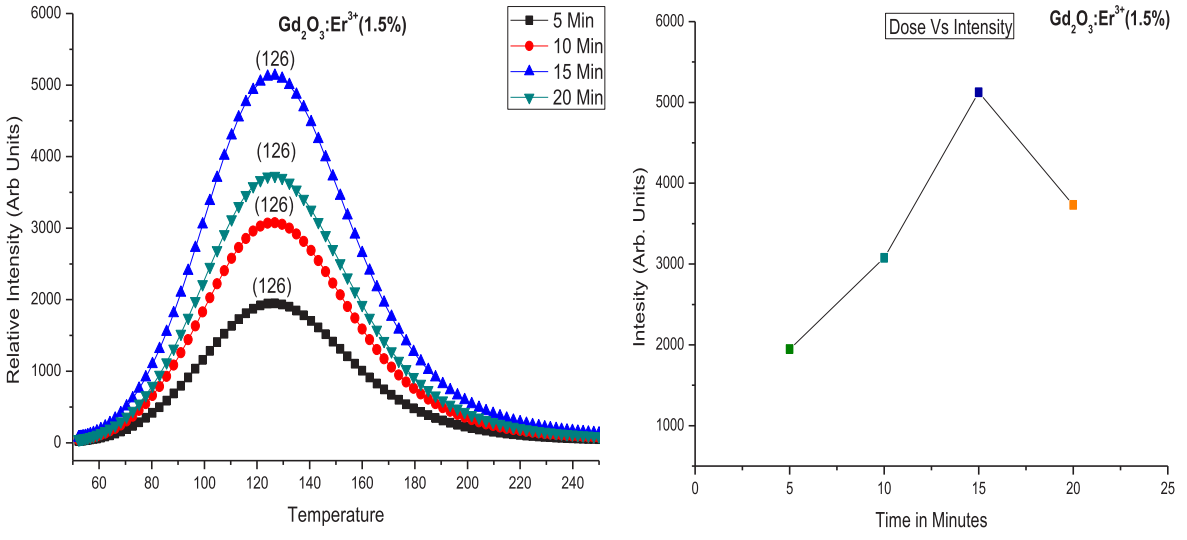


**Fig. 8 – TL glow curve of $Gd_2O_3:Er^{3+}$(1.5%) for different UV exposure time with heating rate 6.7 °C/s.**

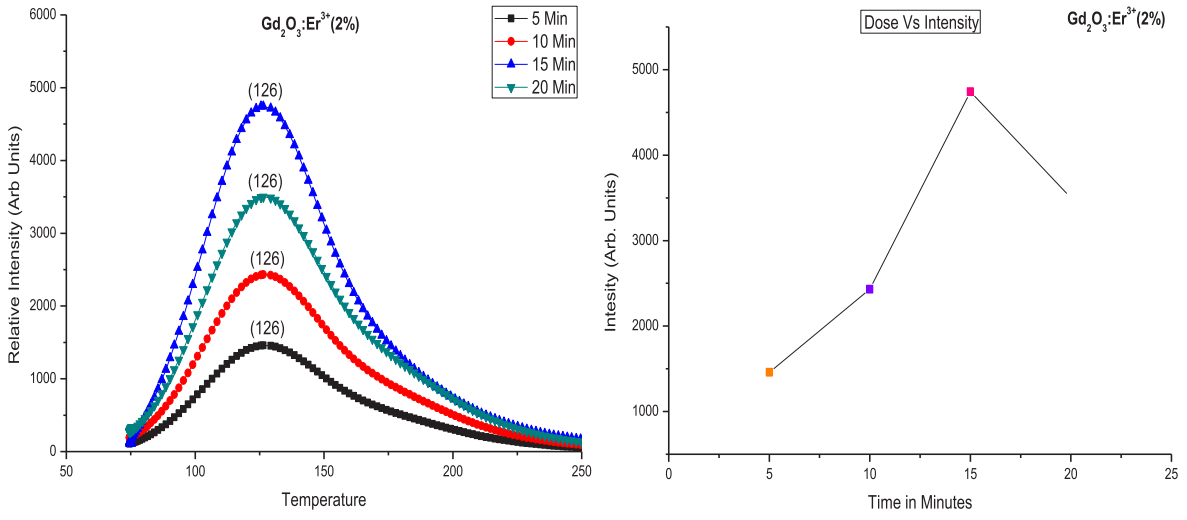


**Fig. 9 – TL glow curve of $Gd_2O_3:Er^{3+}$(2%) for different UV exposure time with heating rate 6.7 °C/s.**

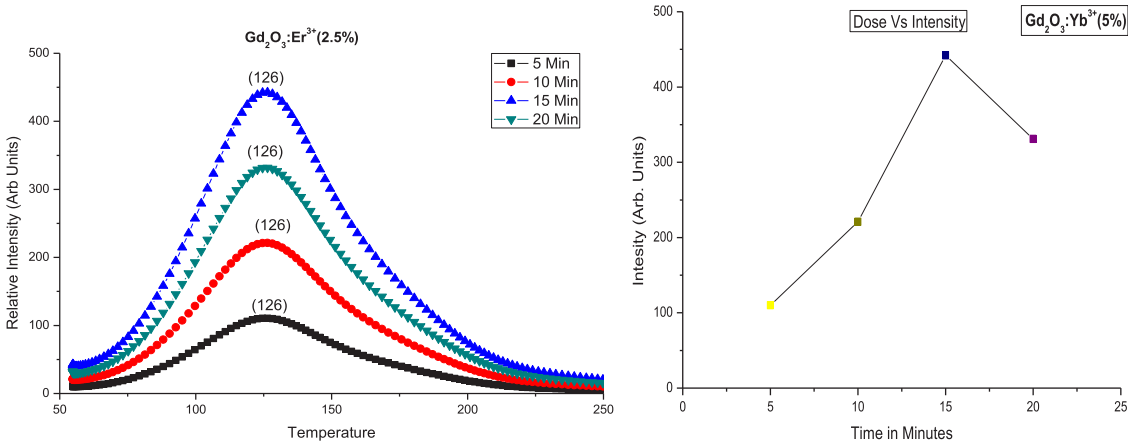


**Fig. 10 – TL glow curve of $Gd_2O_3:Er^{3+}$(2.5%) for different UV exposure time with heating rate 6.7 °C/s.**

**Table 2 – Kinetic parameters of $Gd_2O_3:Er^{3+}$(0.5%) for different UV exposure time with heating rate 6.7 °C/s.**

| UV exposure time | $T_1$ | $T_m$ | $T_2$ | $\tau$ | $\delta$ | $\omega$ | $\mu = \delta/\omega$ | Activation energy E in eV | Frequency factor S in $s^{-1}$ |
|---|---|---|---|---|---|---|---|---|---|
| 5 | 93 | 126 | 160 | 33 | 34 | 67 | 0.50746 | 0.62487 | $9.9 \times 10^8$ |
| 10 | 94 | 126 | 161.5 | 32 | 35.5 | 67.5 | 0.52593 | 0.64839 | $2.05 \times 10^9$ |
| 15 | 93.5 | 126 | 161.2 | 32.5 | 35.2 | 67.7 | 0.51994 | 0.63711 | $1.45 \times 10^9$ |
| 20 | 94.5 | 126 | 160.5 | 31.5 | 34.5 | 66 | 0.52273 | 0.65807 | $2.75 \times 10^9$ |

**Table 3 – Kinetic parameters of $Gd_2O_3:Er^{3+}$(1%) for different UV exposure time with heating rate 6.7 °C/s.**

| UV exposure time | $T_1$ | $T_m$ | $T_2$ | $\tau$ | $\delta$ | $\omega$ | $\mu = \delta/\omega$ | Activation energy E in eV | Frequency factor S in $s^{-1}$ |
|---|---|---|---|---|---|---|---|---|---|
| 5 | 95.8 | 126 | 165.1 | 30.2 | 39.1 | 69.3 | 0.56421 | 0.69613 | $8.8 \times 10^9$ |
| 10 | 94.3 | 126 | 160.2 | 31.7 | 34.2 | 65.9 | 0.51897 | 0.65311 | $2.3 \times 10^9$ |
| 15 | 98.4 | 126 | 159.8 | 27.6 | 33.8 | 61.4 | 0.55049 | 0.7578 | $5.7 \times 10^{10}$ |
| 20 | 94.2 | 126 | 161.2 | 31.8 | 35.2 | 67 | 0.52537 | 0.65238 | $2.3 \times 10^9$ |

Table 2, which shows maximum peak has second order of kinetic for UV irradiated phosphors. The similar response for 1 mol% and higher $Er^{3+}$ doped phosphor were found for the kinetic parameters (Figs. 7–10 and Tables 3–6) the linear response with dose. The intensity increases with increasing UV exposure up to 15 min after that thermal quenching occurs and trap levels destroy. This behaviour of the sample shows high fading and less stability with UV irradiation. The sample shows very good intensity for 15 min UV exposure time and constant heating rate (Chen & Pagonis, 2011). Also the kinetic parameter calculation shows (Tables 3–6) in the similar response and the maximum peaks show the second order of kinetics. The activation energy varies from 0.61 to 0.69 eV for UV irradiated sample. The prepared phosphor is less stable with UV exposure time.

### 4.2. *Effect of $Er^{3+}$ concentration on TL glow curve (concentration quenching)*

The Effect of $Er^{3+}$ concentration on Tl studies were studied by using different $Er^{3+}$ concentration. There intensities were compared and the highest intensity was found for 1% $Er^{3+}$ concentration. (Fig. 11). The concentration quenching occurs when we increase the $Er^{3+}$ concentration above the 1 mol%. The sample shows very good intensity for 15 min UV exposure time and constant heating rate of 6.7 C/Sec (Chen & Pagonis, 2011). Also the kinetic parameter calculation shows (Table 7) in the similar response and the maximum peaks show the second order of kinetics. The activation energy varies from 0.63 to 0.80 eV for different $Er^{3+}$ concentration doped samples.

**Table 4 – Kinetic parameters of $Gd_2O_3:Er^{3+}$(1.5%) for different UV exposure time with heating rate 6.7 °C/s.**

| UV exposure time | $T_1$ | $T_m$ | $T_2$ | $\tau$ | $\delta$ | $\omega$ | $\mu = \delta/\omega$ | Activation energy E in eV | Frequency factor S in $s^{-1}$ |
|---|---|---|---|---|---|---|---|---|---|
| 5 | 94.3 | 126 | 161.3 | 31.7 | 35.3 | 67 | 0.52687 | 0.65476 | $2.4 \times 10^9$ |
| 10 | 95 | 126 | 161.5 | 31 | 35.5 | 66.5 | 0.53383 | 0.67113 | $4.1 \times 10^9$ |
| 15 | 95.5 | 126 | 163.2 | 30.5 | 37.2 | 67.7 | 0.54948 | 0.68574 | $6.4 \times 10^9$ |
| 20 | 96 | 126 | 163 | 30 | 37 | 67 | 0.55224 | 0.69779 | $9.27 \times 10^9$ |

**Table 5 – Kinetic parameters of $Gd_2O_3:Er^{3+}$(2%)for different UV exposure time with heating rate 6.7 °C/s.**

| UV exposure time | $T_1$ | $T_m$ | $T_2$ | $\tau$ | $\delta$ | $\omega$ | $\mu = \delta/\omega$ | Activation energy $E$ in eV | Frequency factor $S$ in $s^{-1}$ |
|---|---|---|---|---|---|---|---|---|---|
| 5 | 99.3 | 126 | 163.5 | 26.7 | 37.5 | 64.2 | 0.584 | 0.792 | $1.6 \times 10^{11}$ |
| 10 | 99.5 | 126 | 161.5 | 26.5 | 35.5 | 62 | 0.573 | 0.795 | $1.8 \times 10^{11}$ |
| 15 | 99.8 | 126 | 159.5 | 26.2 | 33.5 | 59.7 | 0.561 | 0.801 | $2.1 \times 10^{11}$ |
| 20 | 98.5 | 126 | 163.9 | 27.5 | 37.9 | 65.4 | 0.58 | 0.768 | $7.9 \times 10^{10}$ |

**Table 6 – Kinetic parameters of $Gd_2O_3:Er^{3+}$(2.5%) for different UV exposure time with heating rate 6.7 °C/s.**

| UV exposure time | $T_1$ | $T_m$ | $T_2$ | $\tau$ | $\delta$ | $\omega$ | $\mu = \delta/\omega$ | Activation energy $E$ in eV | Frequency factor $S$ in $s^{-1}$ |
|---|---|---|---|---|---|---|---|---|---|
| 5 | 96.3 | 126 | 161.6 | 29.7 | 35.6 | 65.3 | 0.545 | 0.703 | $1.1 \times 10^{10}$ |
| 10 | 96.5 | 126 | 161 | 29.5 | 35 | 64.5 | 0.543 | 0.707 | $1.2 \times 10^{10}$ |
| 15 | 97 | 126 | 162 | 29 | 36 | 65 | 0.554 | 0.722 | $1.9 \times 10^{10}$ |
| 20 | 96 | 126 | 162.5 | 30 | 36.5 | 66.5 | 0.549 | 0.697 | $9.1 \times 10^{09}$ |

### 4.3. *Heating rate effect for UV exposure*

The heating rate effect on TL glow curve for fixed concentration of $Er^{3+}$ (1 mol%) and fixed 15 min UV exposure time was recorded. (Fig. 12). This study shows the peak temperature shifted towards the higher temperature side on increase of heating rate. all the glow curve shows second order of kinetic for variable heating rate studies of $Gd_2O_3:Er^{3+}$(1%) (Table 8). The activation energies vary from 0.63 eV to 0.7 eV, more the heating rate the activation energy also increases. Similar behaviour reported by Dubey et al. For geological sample collected from amaranth holy cave (Dubey, Jagjeet Kaur, Suryanarayana, & Murthy, 2014).

### 4.4. *Gamma dose–response*

Fig. 13 shows the TL glow curves of $Gd_2O_3:Er^{3+}$(1%) exposed to different γ-doses in the range 0.5–2 kGy at a heating rate of 6.7 °C/s. Single TL glow curves was found at 214 °C for all samples. Variation of TL intensity at the glow peaks of 214 °C against different γ-doses was studied and shown in Fig. 13. It can be seen from the figure that, the linearity was observed up to the range from 0.5 to 2 kGy, within this range the material is quite useful as a dosimeter. With further increase in γ-dose, TL intensity increases. Upto the given γ-dose, TL glow curves do not undergo any alteration except increase in intensity. This change in the relative intensity of the glow peaks was mainly attributed to the change in the population of the luminescent/trapping centres. Further, a small shift in TL glow peak positions was observed towards higher temperature side. This was due to different kinds of traps produced by irradiation (Furetta & Weng, 1998; Singh et al., 2011). Here the deep trap formation occurs because the sample irradiated by higher energy gamma rays. In case of UV irradiated sample the lower temperature peak was found which represents the formation of shallow traps (Figs. 6–12). The prepared phosphor is less stable with UV exposure time but it shows opposite behaviour with gamma irradiation in case of gamma irradiation the high temperature peak at 214 °C found (Fig. 13) and it shows continuous increase with gamma dose.

The increase in TL intensity with γ-dose was explained on the basis of track interaction model (TIM). The number of created luminescent traps/centres in $Gd_2O_3:Er^{3+}$(1%) due to γ-irradiation depends on (i) the length and area of cross section of the created track in $Gd_2O_3$ matrix. In case of bulk materials (single crystal/microcrystal), the high energy γ-irradiation could create a track equal to the dimension of the crystallite/crystal in nm range, however in nanostructured material the length of the track was in the order of few tens of nanometre (nm). For lower γ-doses, the number of generated traps/luminescent centres in nanocrystalline

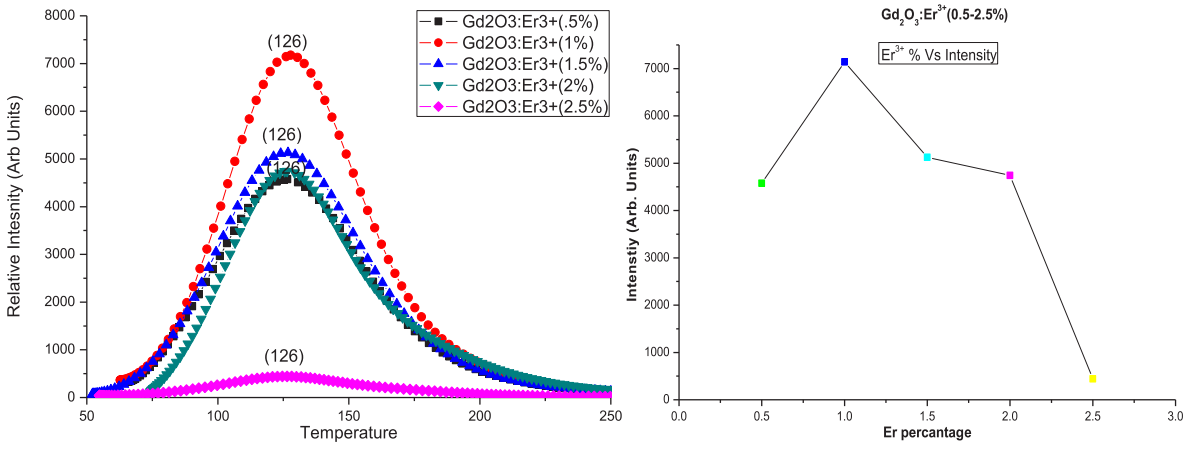


**Fig. 11 – TL glow curve of $Gd_2O_3:Er^{3+}$(0.5–2.5%) for 15 min UV exposure time with heating rate 6.7 °C/s.**

**Table 7 – Kinetic parameters of $Gd_2O_3:Er^{3+}$(0.5–2.5%) for 15 min UV exposure time with heating rate 6.7 °C/s.**

| $Er^{3+}$ percentage | $T_1$ | $T_m$ | $T_2$ | $\tau$ | $\delta$ | $\omega$ | $\mu = \delta/\omega$ | Activation energy E in eV | Frequency factor S in $s^{-1}$ |
|---|---|---|---|---|---|---|---|---|---|
| 0.5 | 93.5 | 126 | 161.2 | 32.5 | 35.2 | 67.7 | 0.51994 | 0.63711 | $1.45 \times 10^9$ |
| 1 | 98.4 | 126 | 159.8 | 27.6 | 33.8 | 61.4 | 0.55049 | 0.7578 | $5.7 \times 10^{10}$ |
| 1.5 | 95.5 | 126 | 163.2 | 30.5 | 37.2 | 67.7 | 0.54948 | 0.68574 | $6.4 \times 10^9$ |
| 2 | 99.8 | 126 | 159.5 | 26.2 | 33.5 | 59.7 | 0.561 | 0.801 | $2.1 \times 10^{11}$ |
| 2.5 | 97 | 126 | 162 | 29 | 36 | 65 | 0.554 | 0.722 | $1.9 \times 10^{10}$ |

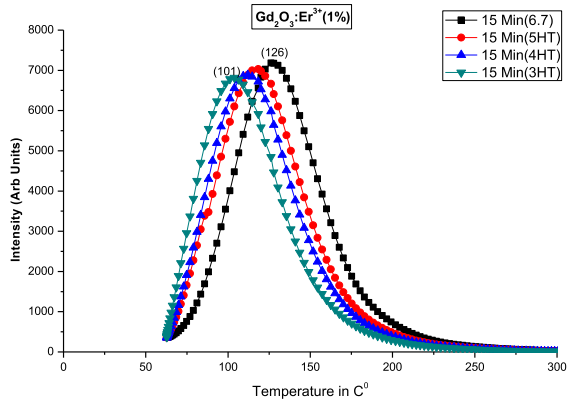


**Fig. 12 – TL glow curve of $Gd_2O_3:Er^{3+}$(1%) for 15 min UV exposure for different heating rate.**

materials would be less than that of bulk material. Further, with increase of $\gamma$ dose, more number of tracks were overlapped in micro-crystalline materials which may not give extra TL, as a result TL intensity decreases. As size of particles was in nm, some of the particles which may have missed while irradiating with higher $\gamma$-dosages. This slows down the process of generating the competing traps at different levels as a result wide range of linearity was expected (Horowitz, Avila, & Rodriguez-Villafuerte, 2001; Mahajna & Horowitz, 1997).

The dosimetric characteristic of the phosphor mainly depends on kinetic parameters namely frequency factor (s), order of kinetics (b) and trap depth (E). These parameters reveal the stability of traps/luminescent centres. If the value of E was low, the glow peak occurs at a relatively lower trap and the corresponding trap created was unstable. As a result the corresponding TL glow peak shows strong fading. If the value of 'S' was high, fading was less. The order of kinetics gives the information about the trapped charge carriers were retrapped on heating or not. Chen's half width method overcomes the geometrical reproducibility and the contact problem of the sample with the heating planchet that apparently alters the kinetics (Chen, 1969; Chen & Kirsh, 1981; Chen, Lawless, & Pagonis, 2011; Chen & Mceever, 1997). The calculation of kinetic parameters for gamma irradiated samples is shown in Tables 9 and 10.

**Table 8 – Kinetic parameters of $Gd_2O_3:Er^{3+}$(1%) for 15 min UV exposure for different heating rate.**

| Heating rate | $T_1$ | $T_m$ | $T_2$ | $\tau$ | $\delta$ | $\omega$ | $\mu = \delta/\omega$ | Activation energy E in eV | Frequency factor S in $s^{-1}$ |
|---|---|---|---|---|---|---|---|---|---|
| 6.7 | 93.5 | 126 | 159.2 | 32.5 | 33.2 | 65.7 | 0.505327 | 0.634174 | $1.32 \times 10^9$ |
| 5 | 88.2 | 118 | 149.2 | 29.8 | 31.2 | 61 | 0.511475 | 0.66586 | $5.38 \times 10^9$ |
| 4 | 83.4 | 111 | 143.5 | 27.6 | 32.5 | 60.1 | 0.540765 | 0.699804 | $2.33 \times 10^{10}$ |
| 3 | 76.8 | 101 | 135.5 | 26.2 | 32.5 | 58.7 | 0.553663 | 0.709649 | $5.21 \times 10^{10}$ |

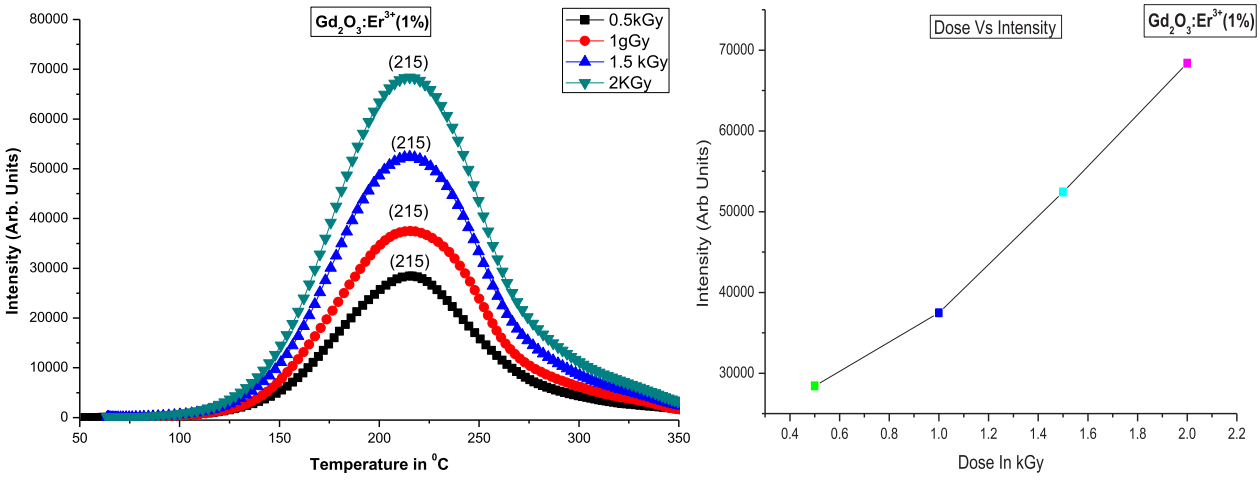


**Fig. 13 – TL glow curve of $Gd_2O_3:Er^{3+}$(1%) for gamma exposure for 6.7 C/s heating rate.**

**Table 9 – Kinetic parameters of $Gd_2O_3:Er^{3+}$(1%) for different gamma exposure for fixed 6.7 C/s heating rate.**

| Dose in kGy | $T_1$ | $T_m$ | $T_2$ | $\tau$ | $\delta$ | $\omega$ | $\mu = \delta/\omega$ | Activation energy E in eV | Frequency factor S in $s^{-1}$ |
|---|---|---|---|---|---|---|---|---|---|
| 0.5 | 174 | 215 | 254 | 41 | 39 | 80 | 0.488 | 0.748 | $5.3 \times 10^8$ |
| 1 | 172.5 | 215 | 257 | 42.5 | 42 | 84.5 | 0.497 | 0.723 | $2.8 \times 10^8$ |
| 1.5 | 171 | 215 | 256.5 | 44 | 41.5 | 85.5 | 0.485 | 0.695 | $1.4 \times 10^8$ |
| 2 | 172 | 215 | 254.5 | 43 | 39.5 | 82.5 | 0.479 | 0.71 | $2.1 \times 10^8$ |

**Table 10 – Kinetic parameters of $Gd_2O_3:Er^{3+}$(1%) for 2 kGy gamma exposure for different heating rate.**

| Heating rate | $T_1$ | $T_m$ | $T_2$ | $\tau$ | $\delta$ | $\omega$ | $\mu = \delta/\omega$ | Activation energy E in eV | Frequency factor S in $s^{-1}$ |
|---|---|---|---|---|---|---|---|---|---|
| 6.7 | 172 | 215 | 254.5 | 43 | 39.5 | 82.5 | 0.478788 | 0.710309 | $2.1 \times 10^8$ |
| 5 | 161.5 | 205 | 247.3 | 43.5 | 42.3 | 85.8 | 0.493007 | 0.676219 | $1.2 \times 10^8$ |
| 4 | 148.2 | 194 | 236.7 | 45.8 | 42.7 | 88.5 | 0.482486 | 0.609917 | $3.4 \times 10^7$ |
| 3 | 141.5 | 186 | 228.4 | 44.5 | 42.4 | 86.9 | 0.487917 | 0.60769 | $4.3 \times 10^8$ |

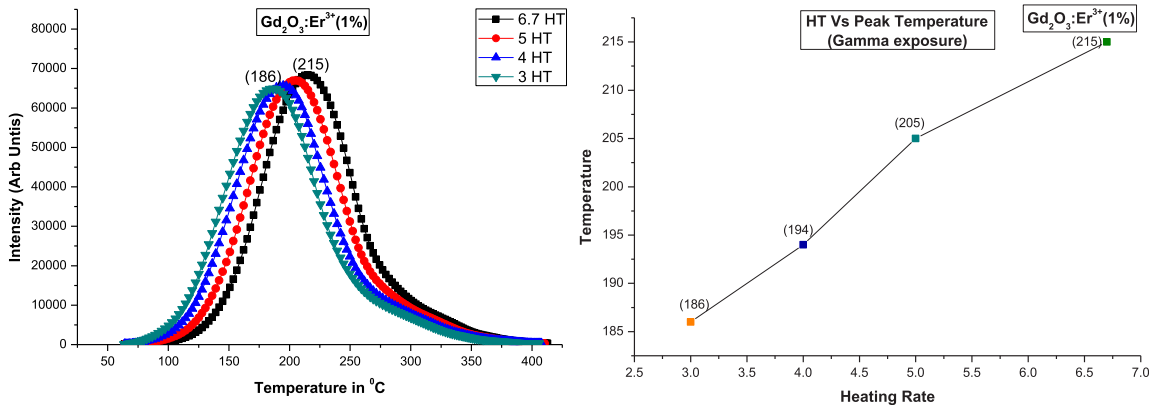


**Fig. 14 – TL glow curve of $Gd_2O_3:Er^{3+}$(1%) for 2 kGy gamma exposure for different heating rate.**

### 4.5. *Heating rate effect for gamma exposure*

Also the heating rate effect of gamma irradiated phosphors shows the linear response with increase in heating rate this is similar to the UV radiation (Fig. 14). The various kinetic parameters were shown in Table 10.

## 5. Conclusion

$Gd_2O_3:Er^{3+}$ doped phosphor was successfully synthesized by solid state reaction method. This method is suitable for large scale production. XRD studies conform the formation of nanophosphor, which are in single phase and cubic structure. In thermoluminescence study maximum peak shows the second order of kinetics means two or more traps formation in the sample. Sample was irradiated by UV and gamma exposure and both exposures compared with TL studies. Here the UV exposed sample shows the high fading and lower stability as compared to gamma exposed sample. The shallow (surface) trap formation for UV irradiated sample shows lower temperature peak. The lower temperature peak is not suitable for thermoluminescence dosimetric application. However for gamma irradiated sample shows the high temperature peak with linear response with dose which indicates that these peaks are suitable and useful for dosimetric applications. The SEM, TEM studies show the formation of nanophosphors with the good surface morphology some defects found because the sample prepared by high temperature synthesis method. The nanocrystalline sample shows the good TL peak due to some defects generated by preparation method. The sample may be useful for dosimetry and for personal monitoring.

## Acknowledgement

We are very grateful to IUC Indore for XRD characterization and also thankful to Dr. Mukul Gupta for his cooperation. I am very thankful to SAIF IIT, Bombay for other characterization such as SEM, TEM, FTIR and EDX.

## REFERENCES

Barghare, S. P., Joshi, R. V., Kathuria, S. P., & Joshi, T. R. (1982). Intrinsic thermoluminescence of NaCl:Tl in UV dosimetry. *Radiation Effects and Defects in Solids, 66*(3–4), 217–222.

Chen, R. (1969). Thermally stimulated current curves with non-constant recombination lifetime. *British Journal of Applied Physics, 2*, 371–375.

Chen, R., & Kirsh, Y. (1981). *The analysis of thermally stimulated processes*. Oxford, New York: Pergamon Press.
Chen, R., Lawless, J. L., & Pagonis, V. (2011). A model for explaining the concentration quenching of thermoluminescence. *Radiation Measurements, 46*, 1380–1384.
Chen, R., & Mceever, S. W. S. (1997). *Theory of thermoluminescence and related phenomena*. London, NJ, Singapore: World Scientific Publications.
Chen, R., & Pagonis, V. (2011). *Thermally and optically stimulated luminescence: A simulation approach*. Chichester: Wiley.
Dubey, V., Jagjeet Kaur, N. S., Suryanarayana, K. V. R., & Murthy. (2014). *Research on Chemical Intermediates*. http://dx.doi.org/10.1007/s11164-012-0980-4.
Falcony, C., Garcia, M., Ortiz, A., & Alonso, C. (1992). Luminescent properties of ZnS: Mn films deposited by spray pyrolysis. *Journal of Applied Physics, 72*, 1525.
Furetta, C., & Weng, P. S. (1998). *Operational thermoluminescence dosimetry*. Singapore: World Scientific Publishing Co., Pvt. Ltd.
Garcia-Murillo, A., Luyer, C. L., Garapon, C., Dujardin, C., Bernstein, E., Pedrini, C., et al. (2002). Optical properties of europium-doped $Gd_2O_3$ waveguiding thin films prepared by the sol–gel method. *Optical Material, 19*(1), 161–168.
Gokce, M., Oguz, K. F., Karali, T., & Prokic, M. (2009). Influence of heating rate on thermoluminescence of $Mg_2SiO_4$: Tb dosimeter. *Journal of Physics D: Applied Physics, 42*(10), 105412.
Grier, D., & Mccarthy, G. (1991). North Dakota state university, Fargo, North Dakota, USA, ICCD Grant-in-Aid.
Guo, H., Dong, N., Yin, M., Zhang, W., Lou, L., & Xia, S. (2004). Visible upconversion in rare earth ion-doped $Gd_2O_3$ nanocrystals. *Journal of Physical Chemistry B, 108*(50), 19205–19209.
Horowitz, Y. S., Avila, O., & Rodriguez-Villafuerte, M. (2001). Theory of heavy charged particle response (efficiency and supralinearity) in TL materials. *Nuclear Instruments and Methods in Physics Research Section B, 184*, 85–112.
Kaur, J., Parganiha, Y., Dubey, V., & Singh, D. (September 2014). *Synthesis, characterization and luminescence behavior of ZrO2:Eu3+, Dy3+ with variable concentration of Eu and Dy doped phosphor, superlattices and microstructures* (Vol. 73, pp. 38–53).
Lawless, J. L., Chen, R., & Pagonis, V. (2009). On the theoretical basis of the duplicitous thermoluminescence peak. *Journal of Physics D: Applied Physics, 42*(155409), 8.
Lochab, S. P., Pandey, A., Sahare, P. D., Chauhan, R. S., Salah, N., & Ranjan, R. (2007). Nanocrystalline $MgB_4O_7$: Dy for high dose measurement of gamma radiation. *Physica Status Solidi (A), 204*(7), 2416–2425.
Lochab, S. P., Sahare, P. D., Chauhan, R. S., Salah, N., Ranjan, R., & Pandey, A. (2007). Thermoluminescence and photoluminescence study of nanocrystalline $Ba_{0.97}Ca_{0.03}SO_4$. *European Journal of Physics D: Applied Physics, 40*(5), 1343.
Mahajna, S., & Horowitz, Y. S. (1997). The Unified Interaction Model applied to the gamma induced supralinearity and sensitisation of peak 5 in LiF: Mg,Ti (TLD-100). *Journal of Physics D: Applied Physics, 30*, 2603–2619.
Mckeever, S. W. S. (1986). *Thermoluminescence of solids*. Cambridge: Cambridge University Press.
Nalwa, H. S. (2000). *Handbook of nanostructured materials and nanotechnology* (Vols. 1–5). San Diego, CA: Academic Press.
Noh, A. M., Amin, Y. M., Mahat, R. H., & Bradley, D. A. (2001). *Radiation Physics and Chemistry, 61*(3), 497–499, 29.
Salah, N., Sahare, P. D., Lochab, S. P., & Kumar, P. (2006). TL and PL studies on $CaSO_4$: Dy nanoparticles. *Radiation Measurements, 41*(1), 40–47.
Salah, N., Sahare, P. D., & Rupasov, A. A. (2007). Thermoluminescence of nanocrystalline LiF: Mg, Cu, P. *Journal of Luminescence, 124*(2), 357–364.
Sahare, P. D., Ranjan, R., Salah, N., & Lochab, S. P. (2007). $K_3Na(SO_4)_2$: Eu nanoparticles for high dose of ionizing radiation. *Journal of Physics D: Applied Physics, 40*(3), 759.
Singh, L., Chopra, V., & Lochab, S. P. (2011). Synthesis and characterization of thermoluminescent $Li_2B_4O_7$ nanophosphor. *Journal of Luminescence, 131*, 1177–1183.
Tamrakar, R. K. (2012). *Studies on absorption spectra of Mn doped CdS nanoparticles*. LAP Lambert Academic Publishing, Verlag, ISBN 978-3-659-26222-7.
Tamrakar, R. K., & Bisen, D. P. (2013). Optical and kinetic studies of CdS: Cu nanoparticles. *Research on Chemical Intermediates, 39*, 3043–3048.
Tamrakar, R. K., Bisen, D. P., & Brahme, N. (2014). Characterization and luminescence properties of $Gd_2O_3$ phosphor. *Research on Chemical Intermediates, 40*, 1771–1779.
Tamrakar, R. K., Bisen, D. P., Robinson, C. S., Sahu, I. P., & Brahme, N. (2014). Ytterbium doped gadolinium oxide ($Gd_2O_3$:$Yb^{3+}$) phosphor: topology, morphology, and luminescence behaviour in Hindawi Publishing Corporation. Article ID 396147 *Indian Journal of Materials Science*, 7. Accepted 4 February 2014.
Tamrakar, R. K., Raunak Bisen, D. P., Upadhyay, K., & Bramhe, N. (2014). Effect of fuel on structural and optical characterization of $Gd_2O_3$:$Er^{3+}$ phosphor. *Journal of Luminescence and Applications, 1*(1), 23–29.
Tiwari, R., Awat, V., Tolani, S., Verma, N., Dubey, V., & Tamrakar, R. K. (2014). Optical behaviour of cadmium and mercury free eco-friendly lamp nanophosphor for display devices. *Results in Physics, 4*, 63–68.
Tiwari, A., Khan, S. A., Kher, R. S., Dhoble, S. J., & Mehta, M. (2011). Thermoluminescence characteristics of inorganically and organically capped ZnS: Cu nanophosphors. *Journal of Luminescence, 131*, 2202–2206.
Vij, D. R. (Ed.). (1993). *Thermoluminescent materials*. NJ: PTR Prentice-Hall.
Weiss, D., Horowitz, Y. S., & Oster, L. (2008). Delocalized recombination kinetic modelling of the LiF: Mg,Ti glow peak 5 thermoluminescence system. *Journal of Physics D: Applied Physics, 41*, 185411. http://dx.doi.org/10.1088/0022-3727/41/18/185411.